Journal of Marine Science and Application (2019) 18:522–529
https://doi.org/10.1007/s11804-019-00106-5

RESEARCH ARTICLE

A Space-Time Reverberation Model for Moving Target Detection

Jingwei Yin [1,2,3] · Bing Liu [1,2,3] · Guangping Zhu [1,2,3] · Xiao Han [1,2,3]

Received: 26 June 2018 / Accepted: 2 January 2019 / Published online: 21 October 2019

Abstract
In recent years, moving target detection methods based on low-rank and sparse matrix decomposition have been developed, and they have achieved good results. However, there is not enough interpretation to support the assumption that there is a high correlation among the reverberations after each transmitting pulse. In order to explain the correlation of reverberations, a new reverberation model is proposed from the perspective of scattering cells in this paper. The scattering cells are the subarea divided from the detection area. The energy fluctuation of a scattering cell with time and the influence of the neighboring cells are considered. Key parameters of the model were analyzed by numerical analysis, and the applicability of the model was verified by experimental analysis. The results showed that the model can be used for several simulations to evaluate the performance of moving target detection methods.

Keywords Space-time reverberation · Model scattering cell · Energy fluctuation · Moving target detection

1 Introduction

Moving target detection in reverberant environments has been a challenge for a long time (Zhu et al. 2012; Pan et al. 2014; Khorshidi 2014; Yu and Piao 2016; Yu et al. 2017; Lee et al. 2017). Based on the low-rank and sparse theory (Zhou et al. 2011; Halko et al. 2011; Candès et al. 2011; Chandrasekaran et al. 2011), Li et al. (2012) and Ge et al. (2017) achieved detection (Weichang et al. 2012; Ge et al. 2017) and proved the feasibility of their methods using experiments. In a previous study, we as well introduced another method based on the low-rank and sparse theory and obtained better results (Yin et al. 2018). These methods all assume that a high correlation exists among the reverberations after each transmitting pulse. However, there is no adequate explanation for such assumption yet. Moreover, the performances of these methods were not effectively evaluated, as evaluation through a large number of experiments is not practical; it will cost much and the signal to reverberation ratio is uncontrollable. Therefore, a model is needed to reveal the characteristics of reverberation and describe the reverberation process.

A number of reverberation models have been developed. In recent years, research on reverberation model has mainly been concentrated on shallow water, such as the normal mode model (Grigor'ev et al. 2004; Shang et al. 2008), energy-flux model (Harrison 2003; Wu et al. 2010; Zhou and Zhang 2013), spectral representation model (Lingevitch et al. 2002), and PE model (Saintval and Hayward 2011). Unfortunately, these models do not focus on the correlation among the reverberations after a few transmitting pulses. The purpose of this paper is to build a model that explains the correlation among the reverberations after each transmitting pulse. The model is developed from the perspective of scattering cells. We consider the energy fluctuation of a scattering cell as a stochastic process that is a superposition of its energy fluctuation and the effects of neighboring cells. Reverberation in the model varies with time and space, which is very suitable to simulate the target detection process. Therefore,

Article Highlights
- In order to explain the correlation of reverberations and evaluate the performance of moving target detection methods, a suitable reverberation model must be guaranteed.
- A new reverberation model is proposed from the perspective of scattering cells in which spatial and temporal of the scattering cells were considered.
- The applicability of our model was verified by experimental analysis.

✉ Guangping Zhu
guangpingzhu@hrbeu.edu.cn

[1] Acoustic Science and Technology Laboratory, Harbin Engineering University, Harbin 150001, China

[2] College of Underwater Acoustic Engineering, Harbin Engineering University, Harbin 150001, China

[3] Key Laboratory of Marine Information Acquisition and Security, Harbin Engineering University, Ministry of Industry and Information Technology, Harbin 150001, China

the performance of moving target detection methods can be evaluated.

The rest of the paper is organized as follows. In Section 2, we describe the model with parameters and explain the correlation. We also describe the steps to produce reverberation and present an example of reverberation. The effects of the parameters are discussed in Section 3. Section 4 presents the results of conducted experiments, which verify the reverberation model. Finally, conclusions are presented in Section 5.

2 Model Description

For a frame of beamforming data, each element in the matrix corresponds to a subarea of the detection area. Each subarea is called a scattering cell. The scattering cell contains the volume, surface, and bottom. In this paper, we only consider the first scattering. The model geometry and the correspondence between the scattering cells and elements of the beamforming data are shown in Fig. 1.

The sonar is located in the point at the middle of the Z-axis in the left of Fig. 1. We divide the detection area into $M \times N$ subarea. The blue element in the right of Fig. 1 corresponds to the energy of the blue scattering cell in the left of the figure, and likewise do the other elements. In the figure, r is the range between the sonar and the blue cell in the distance direction, Δr is the length of the blue cell in the distance direction, and $\Delta\theta$ is the angle of the blue cell in the θ direction.

2.1 Fluctuation of Reverberation Energy with Time

It is assumed that each scattering cell contains many scatterers and each scatterer has the same scattering characteristic. Therefore, the backward scattering signal caused by the pth scattering cell can be represented as

$$R_p(t) = \mathrm{Re}\left\{ \sum_{i=1}^{Q_p(t)} b_i\, s(t-\tau_i) \mathrm{e}^{\mathrm{j}\,2\pi\varphi_i t} \right\}$$

where $Q_p(t)$ is the number of scatterers at the moment t; b_i is the complex amplitude of the ith scatterer and only depends on the scattering properties of the ith scatterer; $s(t)$ is the transmitting signal; $\tau_i = 2r_i/c$ is the delay, where r_i is the distance between the sonar and the ith scattering cell, and c is the acoustic velocity in the water; and φ_i is the Doppler shift. According to the central limit theorem, the instantaneous value of the pth cell backward scattering signal follows Gaussian distribution. We express it as a discrete version:

$$R_p[t_i] \sim N\left(\mu_p, \sigma_p^2\right)$$

where t_i is the sequence number of the ith sampling, μ_p is the expectation of the Gaussian distribution, and σ_p^2 is the variance of the Gaussian distribution.

Considering

$$R_p'[t_i] = \frac{R_p[t_i] - \mu_p}{\sigma_p} \tag{1}$$

then

$$R_p'[t_i] \sim N(0,1)$$

Considering

$$E_p[k] = \sum_{i=1}^{T} \left(R_p'[t_i]\right)^2 \tag{2}$$

where k is the number of the transmitting pulse, and T is the length of the reverberation.

Thus $E_p[k]$ follows a chi-square distribution at the degrees of freedom T.

$$E_p[k] \sim \chi^2(T) \tag{3}$$

Let the energy of the pth scattering cell after the kth transmitting pulse be given as

$$A_p[k] = \sum_{t_i=1}^{T} \left(R_p[t_i]\right)^2 \tag{4}$$

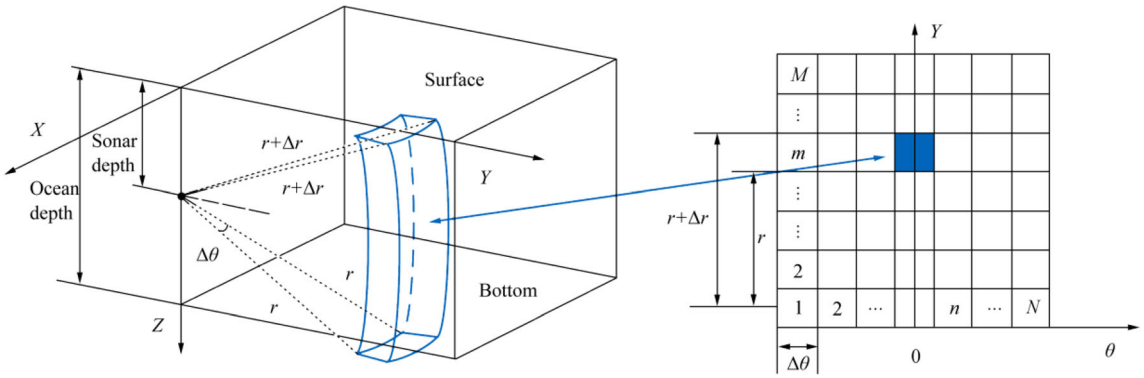

Fig. 1 An element of the matrix corresponding to a subarea

In general, the average of the transmitting signal is 0; thus, we consider $\mu_p = 0$. From Eqs. (1–4), we have

$$A_p[k] \sim \sigma_p^2 \chi^2(T)$$

This shows that we can obtain the energy fluctuation of the pth scattering cell if the variance and the length of the backward scattering signal are known.

2.2 Fluctuation of Reverberation Energy with Space

In fact, the energy of a scattering cell always partly superposes the adjacent scattering cells. As a result, a correlation exists between adjacent scattering cells in terms of energy. For convenience, we ignore the propagation loss associated with distance. It can be regarded as the result of the auto gain control.

Define the energy distribution matrix as

$$\overline{\boldsymbol{A}} = \begin{bmatrix} \sigma_{11}^2 & \sigma_{12}^2 & \cdots & \sigma_{1N}^2 \\ \sigma_{21}^2 & \ddots & & \vdots \\ \vdots & & \ddots & \vdots \\ \sigma_{M1}^2 & \cdots & \cdots & \sigma_{MN}^2 \end{bmatrix}$$

where σ_{mn}^2 is the variance of the (m, n)th scattering cell reverberation, and $\overline{\boldsymbol{A}}$ is related to the scattering properties of the detection area. We can get the energy fluctuation of the (m, n)th scattering cell as

$$A_{mn}[k] \sim \sigma_{mn}^2 \chi^2(T)$$

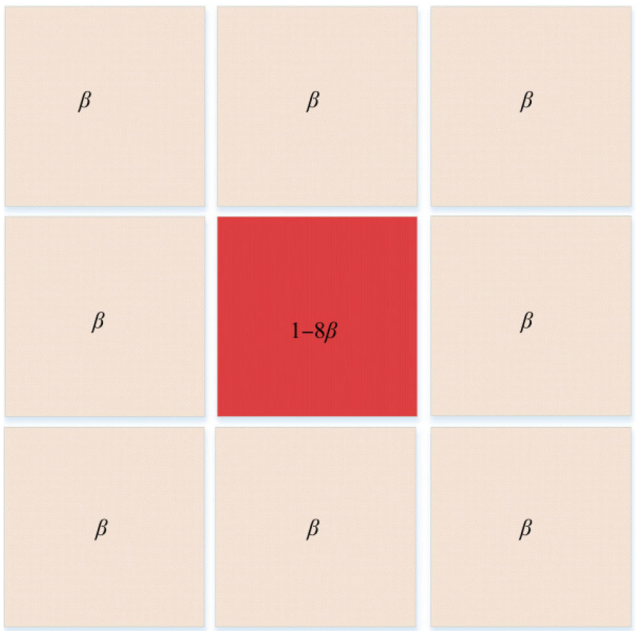

Fig. 2 Energy distribution of one cell

The neighboring scattering cells are assumed to have the same effect on the central scattering cell. The effect is described by the coefficient β. The normalized energy distribution of a scattering cell is presented in Fig. 2. The effect of a type of scattering cell on the neighboring scattering cells is presented in Fig. 3.

Considering the effect as an additive effect, the energy of the (m, n)th scattering cell after the kth transmitting pulse is described as

$$B_{mn}[k] = \beta \sum_{i=m-1}^{m+1} \sum_{j=n-1}^{n+1} A_{ij}[k] + (1-9\beta) A_{mn}[k] \quad (1 \le m \le M, 1 \le n \le N) \tag{5}$$

where $0 \le \beta \le 1/9$. and

$$A_{ij}[k] = \begin{cases} A_{ij}[k] & , \quad 1 \le i \le M, 1 \le j \le N \\ 0 & , \quad else \end{cases}$$

As β changes, the energy fluctuations of the scattering cell are observed to no longer strictly follow a chi-square distribution. We generally consider $0 \le \beta \le 1/16$, because not more than half of the energy of a scattering cell is added to neighboring scattering cells.

2.3 An Example of Reverberation Process

Let $\beta = 0.05$, $T = 100$, and $\overline{\boldsymbol{A}}$ follow a Rayleigh distribution whose expectation is 100. A series of continuous reverberation can be modeled following the steps:

1) Build a matrix $\overline{\boldsymbol{A}} \in \mathbb{R}^{M \times N}$ subjecting to a distribution;
2) Build $M \times N$ vectors of K dimensions subjecting to chi-square distribution, and the (m, n)th vector is described as:

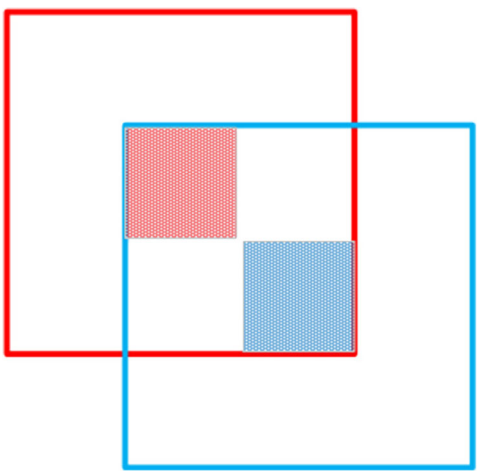

Fig. 3 Effect of the neighboring cell

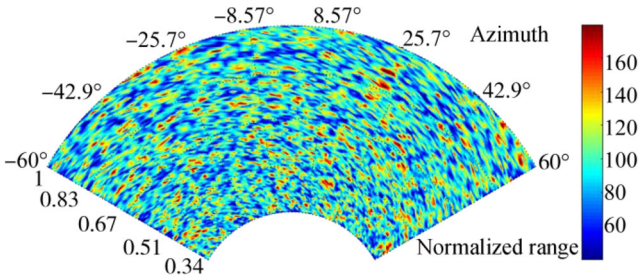

Fig. 4 Example of one frame reverberation

$$\boldsymbol{E}_{mn} = [E_{mn}[1], E_{mn}[2], \cdots, E_{mn}[k], \cdots, E_{mn}[K]]$$

3) Calculate the energy of the (m, n)th scattering cell each frame, respectively;

$$\boldsymbol{A}_{mn} = \sigma_{mn}^2 \boldsymbol{E}_{mn}$$

4) Calculate $\boldsymbol{B}_{mn} \in \mathbb{R}^{1 \times K}$ from Eq. (5);

5) Combine the $\boldsymbol{B}_{mn}$ to $B \in \mathbb{R}^{M \times N \times K}$, whose elements represent the energy of scattering cells in K frames.

A frame of the reverberation is shown in Fig. 4. The radial axis represents the normalized distance, and the tangential axis represents the horizontal azimuth.

3 Numerical Analysis

The model has been introduced in the previous section. The effect of energy distribution matrix $\overline{\boldsymbol{A}}$ and the coefficient β is discussed in this section.

The energy deviation at the kth frame is defined as

$$e[k] = \lg\left[\sum_{m=1}^{M}\sum_{n=1}^{N}\left(B_{mn}[k] - \frac{\overline{A_{mn}}}{S}\right)^2\right]$$

where

$$S = \sum_{m=1}^{M}\sum_{n=1}^{N}\overline{A_{mn}}$$

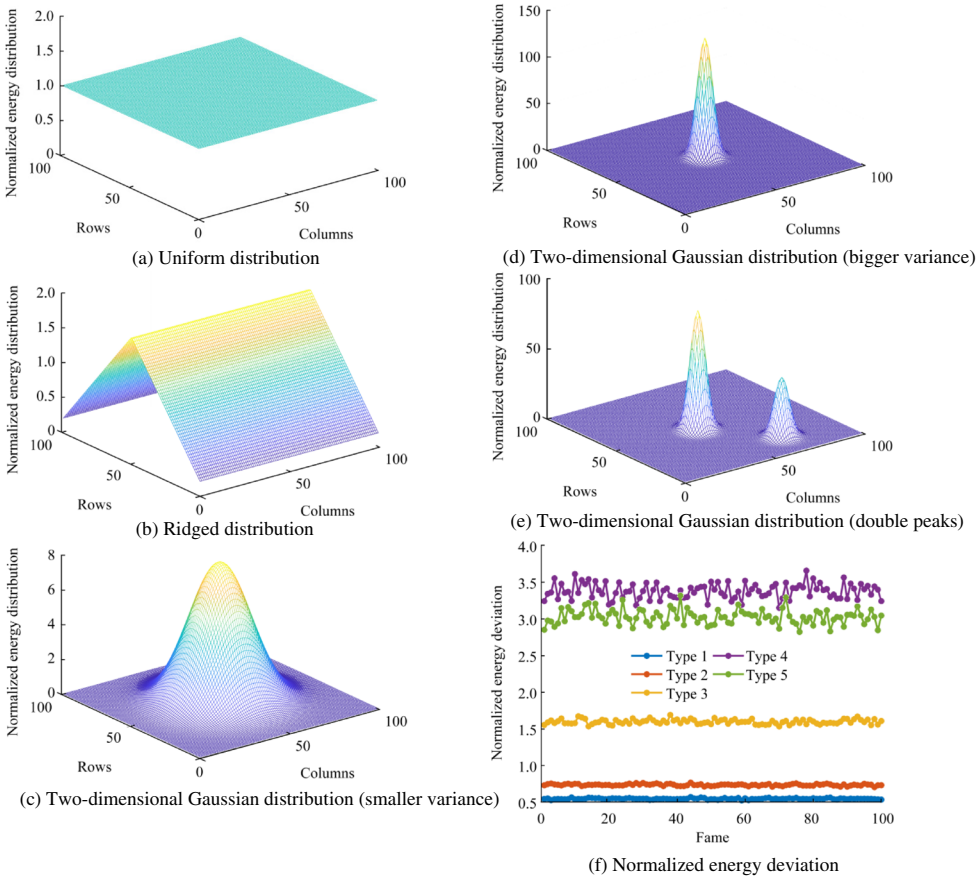

(a) Uniform distribution

(b) Ridged distribution

(c) Two-dimensional Gaussian distribution (smaller variance)

(d) Two-dimensional Gaussian distribution (bigger variance)

(e) Two-dimensional Gaussian distribution (double peaks)

(f) Normalized energy deviation

Fig. 5 Energy distribution and normalized energy deviation

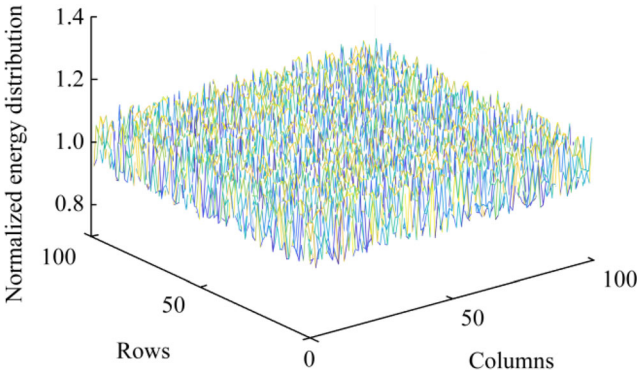

Fig. 6 Normalized energy distribution

For the analysis, five matrices $\overline{\boldsymbol{A}} \in \mathbb{R}^{100\times100}$ were built. Let $\beta = 0$. Their normalized energy distributions are as shown in Fig. 5(a)–(e). The energy distribution is uniform in Fig. 5(a). In Fig. 5(b), the energy distribution is ridged and has a slope of 0.016. The bulged parts of energy in Fig. 5(c)–(e) follow a two-dimensional Gaussian distribution. Their ratio of standard deviation is 4:1:1. The ratio of the two peaks in Fig. 5(e) is 2:1. Figure 5(f) is the normalized energy deviation of each frame. The simulation results show that the more concentrated the energy distribution, the stronger the energy fluctuation of each frame and the lower the correlation of each frame.

As shown in Fig. 5(f), the normalized energy deviations in each frame were stable even though there were fluctuations in the frames. Hence, we discuss the effect of β on the average of the normalized energy deviation, which is

$$e = \frac{1}{K}\sum_{k=1}^{K} e[k] \tag{6}$$

A matrix $\overline{\boldsymbol{A}}$ of uniform distribution was built as shown in Fig. 6. Then e was calculated using Eq. (6). Figure 7 shows that e decreased with increasing β. Figures 2, 3, and 7 indicate the following:

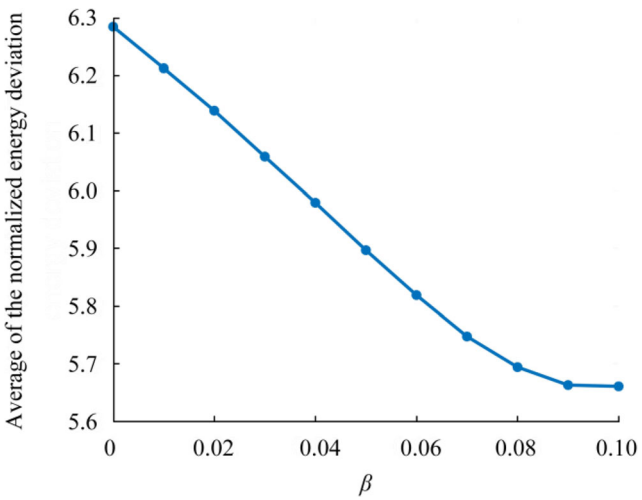

Fig. 7 Average of the normalized energy deviation varying with β

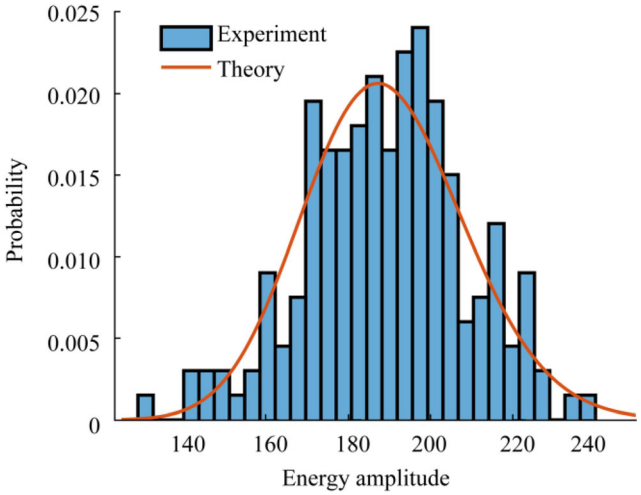

Fig. 8 Energy probability density of a scattering cell

1) When $\beta = 0$, no energy of the cell is added to the neighboring cells; therefore, the e of $\boldsymbol{B}_{mn}$ equals the e of $\boldsymbol{A}_{mn}$. In this case, e is maximum.
2) When $0 < \beta < 1/9$, a fraction of the energy of the cell is added to the neighboring cells; $\boldsymbol{B}_{mn}$ is meant by neighboring cells, but $\boldsymbol{A}_{mn}$ is still the principal component. In this case, e decreases gradually.
3) When β equals 1/9 near 0.1, $\boldsymbol{B}_{mn}$ is the average of the (m, n)th and neighboring cells. In this case, e is meant at the maximum extent and is therefore minimum.

4 Model Matching

To verify whether the model conforms to the actual situation, an experiment of reverberation was performed in the Songhua River in September 2017. A scattering cell in the beamspace was chosen, and its data was normalized with the variance equaling 1. Its probability density is as shown in Fig. 8. The column diagram represents the probability density of the experimental data, and the line represents the probability density of chi-square distribution. Their trends are majorly the same, but not a perfect match.

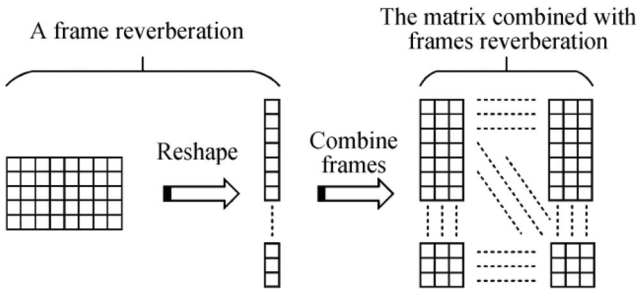

Fig. 9 Matrix combination

Fig. 10 Results of 2D-FT

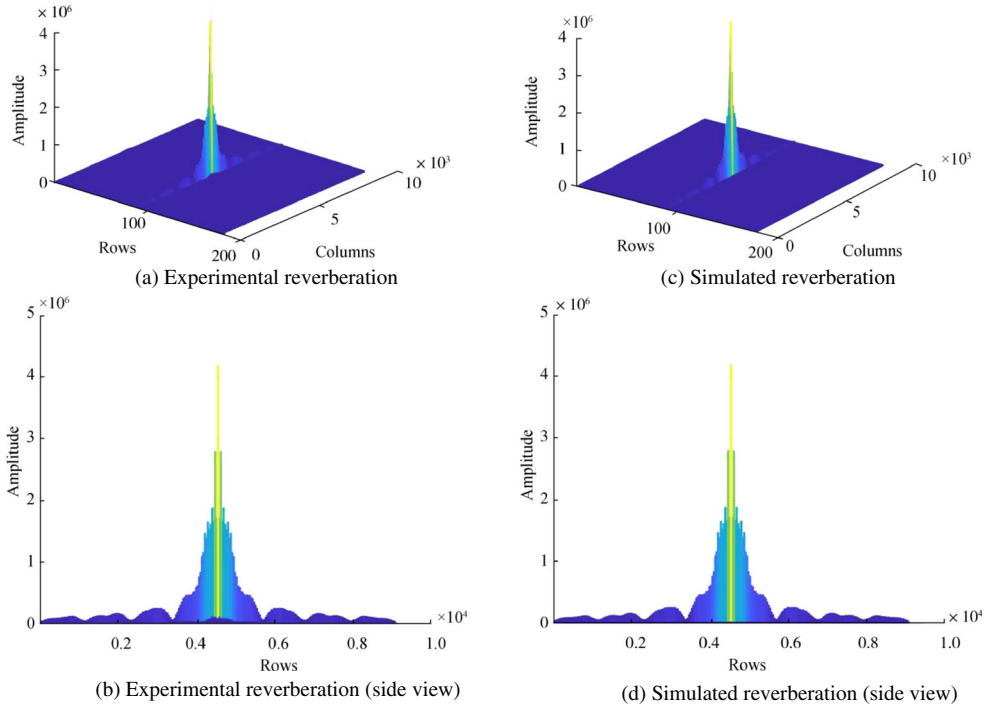

Measurement error, environment noise, lack of samples, and the effect of the neighboring cells may be the reasons the experimental data did not accurately follow the chi-square distribution. If the energy of a neighboring scattering cell is much larger than that of the central cell, the effect will be very significant.

In practice, $\overline{\boldsymbol{A}}$ and β cannot be measured. We considered $\beta = 0$ to calculate approximately; thus, we obtained $\overline{\boldsymbol{A}}$ by calculating the average of each cell energy over 180 frames. We evaluated the matching degree of the model by calculating the two-dimensional Fourier transform (2D-FT). First, we reshaped the experimental reverberation matrix of the 180

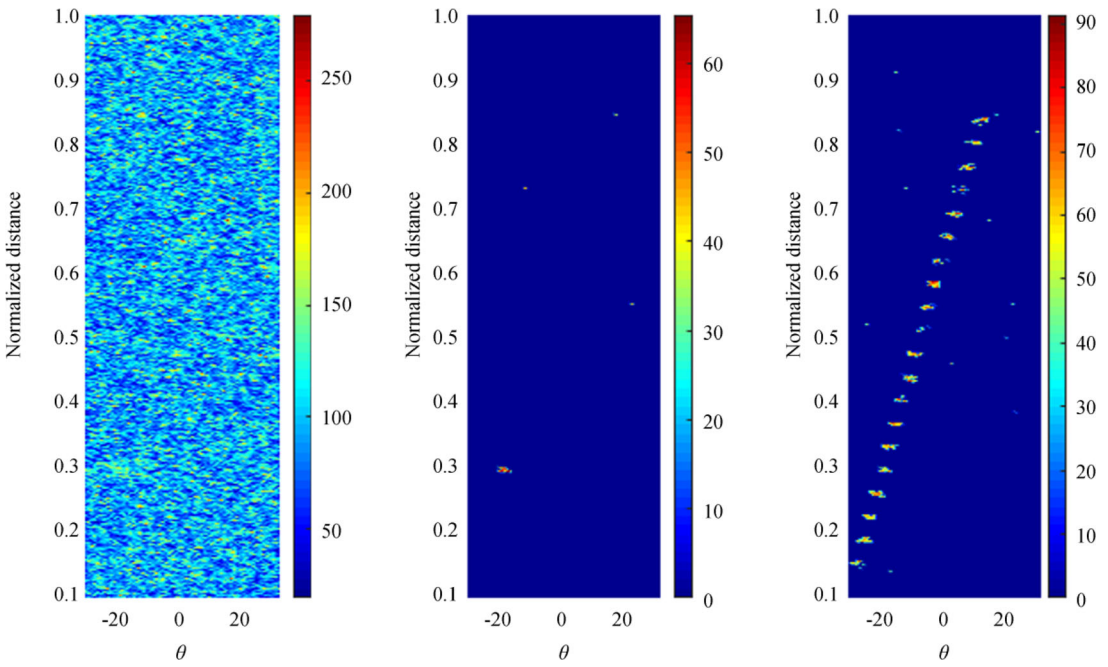

Fig. 11 Example of moving target detection

frames to vectors and combined the 180 vectors to a matrix $\boldsymbol{C}_e \in \mathbb{R}^{MN \times 180}$, which is shown in Fig. 9. Second, we obtained $\boldsymbol{C}_s \in \mathbb{R}^{MN \times 180}$ from the simulated reverberation. Finally, we evaluated the matching degree by

$$e_{\text{match}} = \sum_{m=1}^{M}\sum_{n=1}^{N}\{[\text{FT2}(\boldsymbol{C}_e)-\text{FT2}(\boldsymbol{C}_s)]\circ[\text{FT2}(\boldsymbol{C}_e)-\text{FT2}(\boldsymbol{C}_s)]^*\}/\sum_{m=1}^{M}\sum_{n=1}^{N}\left[\text{FT2}(\boldsymbol{C}_e)\circ\text{FT2}(\boldsymbol{C}_e)^*\right]$$

where FT2(·) is to calculate the 2D-FT of a matrix, ∘ represents the element-wise product, and $(\cdot)^*$ represents the complex conjugate. The smaller the matching error e_{match}, the higher the degree of model matching.

To observe the results of model matching more intuitively, we show the results as Fig. 10. Figure 10(a) is the 2D-FT result of experimental reverberation. Figure 10(b) is the side view of Fig. 10(a). Figure 10(c) is the 2D-FT result of simulated reverberation. Figure 10(d) is the side view of Fig. 10(c). As shown in Fig. 10, the 2D-FT results of the experimental and simulated reverberation are very similar. At this moment, $e_{\text{match}} = 0.35$.

We used the model to simulate the process of moving target detection based on the low-rank and sparse theory. A target was added in each frame of the reverberation at continuous positions, and then the moving target was detected using Ge's method (Ge et al. 2017). The result is shown in Fig. 11. Figure 11(a) shows a frame data mixed with reverberation and a target. Figure 11(b) presents the result of detection corresponding to Fig. 11(a). Figure 11(c) shows the trajectory of the moving target in 20 frames. The result is similar to that in Ge et al. (2017). The experimental findings show that the model can be applied to the simulation of moving target detection.

5 Conclusions

In this study, we develop a new reverberation model considering the reverberation energy. The cell energy fluctuation with time and the effect of the neighboring cells are considered. We discuss the key parameters of the model. The model is simple and practical and explains the high correlation of the reverberations after each transmitting pulse. We used the model to fit the experimental data and present an example to show the feasibility and practicability of the model for moving target detection. We only considered the statistical characteristics of the energy fluctuation of scattering cells over a period of time. The continuous characteristics of the energy fluctuation between two frames will be studied in our future work.

Funding This study was supported by the National Natural Science Foundation of China (Grant Nos. 61631008, 61471137, 50509059, and No.51779061), the Fok Ying-Tong Education Foundation, China (Grant No. 151007), and the Heilongjiang Province Outstanding Youth Science Fund (JC2017017).

References

Candès EJ, Li X, Ma Y, Wright J (2011) Robust principal component analysis. J ACM 58(3):1–37. https://doi.org/10.1145/1970392.1970395

Chandrasekaran V, Sanghavi S, Parrilo PA, Willsky AS (2011) Rank-sparsity incoherence for matrix decomposition. SIAM J Optim 21(2):572–596. https://doi.org/10.1137/090761793

Ge FX, Chen Y, Li W (2017) Target detecton and tracking via structured convex optimization. 2017 IEEE International Conference on Acoustics, Speech and Signal Processing (ICASSP), New Orleans, pp 426–430

Grigor'ev VA, Kuz'kin VM, Petnikov BG (2004) Low-frequency bottom reverberation in shallow-water ocean regions (article). Acoust Phys 50(1):37–45. https://doi.org/10.1134/1.1640723

Halko N, Martinsson PG, Tropp JA (2011) Finding structure with randomness: probabilistic algorithms for constructing approximate matrix decompositions. SIAM Rev 53(2):217–288. https://doi.org/10.1137/090771806

Harrison CH (2003) Closed-form expressions for ocean reverberation and signal excess with mode stripping and Lambert's law. J Acoust Soc Am 114(5):2744–2756. https://doi.org/10.1121/1.1618240

Khorshidi S (2014) The principal component inverse algorithm for detection in the presence of reverberation using autoregressive model. Iran J Sci Technol-Trans Electr Eng 38(E1):91–97. https://doi.org/10.22099/IJSTE.2014.2100

Lee DH, Shin JW, Do DW, Choi SM, Kim HN (2017) Robust LFM target detection in wideband sonar systems. IEEE Trans Aerosp Electron Syst 53(5):2399–2412. https://doi.org/10.1109/TAES.2017.2696318

Li W, Subrahmanya N, Xu F (2012) Online subspace and sparse filtering for target tracking in reverberant environment. Proceedings of the IEEE Sensor Array and Multichannel Signal Processing Workshop (2):329–332. https://doi.org/10.1109/SAM.2012.6250502

Lingevitch JF, Song HC, Kuperman WA (2002) Time reversed reverberation focusing in a waveguide. J Acoust Soc Am 111(6):2609–2614. https://doi.org/10.1121/1.1479148

Pan X, Li CX, Xu YX, Xu W, Gong XY (2014) Combination of time-reversal focusing and nulling for detection of small targets in strong reverberation environments. IET Radar Sonar Navig 8(1):9–16. https://doi.org/10.1049/iet-rsn.2012.0359

Saintval WJ, Hayward TJ (2011) Modulation of a high-frequency shallow-water acoustic channel by sea surface waves: 3-D PE-based modeling. OCEANS 2011 IEEE - Spain, Santander, pp 1–6

Shang EC, Gao T, Wu J (2008) A shallow-water reverberation model based on perturbation theory. IEEE J Ocean Eng 33(4):451–461. https://doi.org/10.1109/JOE.2008.2001686

Weichang L, Subrahmanya N, Feng X (2012) Online subspace and sparse filtering for target tracking in reverberant environment. 2012 IEEE 7th Sensor Array and Multichannel Signal Processing Workshop (SAM), Hoboken, pp 329–332

Wu JR, Shang EC, Gao TF (2010) A new energy-flux model of waveguide reverberation based on perturbation theory. J Comput Acoust 18(03):209–225

Yin J, Liu B, Zhu G, Xie Z (2018) Moving target detection using dynamic mode decomposition. Sensors 18(10):3461. https://doi.org/10.3390/s18103461

Yu G, Piao SC (2016) Multiple moving targets detection and parameters estimation in strong reverberation environments. Shock Vib, Article ID 5274371 2016:1–10. https://doi.org/10.1155/2016/5274371

Yu G, Piao SC, Han X (2017) Fractional Fourier transform-based detection and delay time estimation of moving target in strong reverberation environment. Iet Radar Sonar Navig 11(9):1367–1372. https://doi.org/10.1049/iet-rsn.2016.0601

Zhou JX, Zhang XZ (2013) Integrating the energy flux method for reverberation with physics-based seabed scattering models: modeling and inversion. J Acoust Soc Am 134(1):55–66. https://doi.org/10.1121/1.4807562

Zhou T, Tao D, Wu X (2011) Manifold elastic net: a unified framework for sparse dimension reduction. Data Min Knowl Disc 22(3):340–371

Zhu QY, Li YC, Jiang YL (2012) Line-type moving object detection for sonar images. In: Zhang WJ, Yang XK, Xu ZX, An P, Liu QZ, Lu Y (eds) Advances on digital television and wireless multimedia communications. Springer-Verlag Berlin, Berlin, pp 189–196